Lattice dynamics and specific heat of α-helical poly(*L*-alanine)[a)]

Vandana K. Datye and S. Krimm
Biophysics Research Division, University of Michigan, Ann Arbor, Michigan 48109

(Received 4 February 1986; accepted 10 March 1986)

We have calculated the phonon dispersion relation in α-poly(*L*-alanine) with all atoms in the chemical repeat explicitly included and using a recently refined force field for the polypeptide chain. The phonon density of states shows very good agreement with the inelastic neutron scattering data for this polypeptide. The specific heat for $T < 150$ K yields better agreement with experiment than did earlier calculations. At higher temperatures the discrepancy with experiment remains. We present a simple model calculation which suggests that the source of this discrepancy may lie in the anharmonicity of the methyl torsion mode.

INTRODUCTION

As part of a program to develop transferable force fields for the polypeptide chain that can be used in vibrational analyses of conformation,[1] we have recently refined a force field for α-helical poly(*L*-alanine).[2] In this analysis, all atoms in the chemical repeat unit, $[NH–CH(CH_3)–CO]_n$, were included, in distinction to earlier calculations[3–5] in which the CH_3 group was treated as a point mass. The normal mode frequencies obtained from this calculation were found to be in better agreement with observed infrared and Raman bands[2] than had been the case for the previous calculations.[3–5]

While this improved agreement with optical frequencies suggests a greater validity for this force field,[3] it is also important to know how well the force field predicts other physical properties that depend on the vibrational spectrum, such as the inelastic neutron scattering (INS) cross section and the specific heat. The reason is that, in a crystal, while the optical properties are determined by the phonon spectrum at the center of the Brillouin zone (B.Z.), the other properties depend on the complete phonon dispersion relation and thus can provide a more detailed test of the force field. Since data are available on the neutron scattering spectrum[6,7] and on the specific heat[8] of α-poly(*L*-alanine), we have undertaken calculations designed to provide comparisons with these observations. We also hoped to shed some light on the nature of the discrepancy for $T \geqslant 150$ K between the calculated[5] and observed[8] specific heats, and in particular on whether this was due to the side-chain point-mass approximation.

The phonon density of states that we calculate from the normal modes of the infinite helix is in good agreement with the observed neutron scattering spectra. Although the specific heat discrepancy still exists, our calculations suggest that anharmonicity of the methyl torsion mode may be responsible for this difference. We find that, except for the low-lying CH_3 torsion mode, branches arising from CH_3 group vibrations are nondispersive, thus making the side-chain point-mass approximation valid except in the low-frequency region.

We also report calculations of normal modes of finite helices of varying length, which we have undertaken in order to study the influence of finite size on the density of states and on the specific heat. These calculations were done in the side-chain point-mass approximation, which is an adequate approximation for this purpose.

CALCULATIONS

Model

In all cases, calculations were done on regular isolated helices. The structural parameters were those used previously,[2] and correspond to the 47_{13} helix refined from x-ray studies[9]: the dihedral angles are $\phi = -57.37°$, $\psi = -47.49°$, and h (rise/residue) $= 1.495$ Å. In the case of the finite helix, the end groups were taken as NH_3^+ (assumed to be a point mass) and CO_2^-, with the side chain taken as a point mass of 15 units.

The force field for the full calculation was the same as that used previously.[2] It should be noted that it includes hydrogen-bond force constants explicitly. The force field for the CH_3 point-mass cases was one refined from the full force field specifically for this approximation,[10] and gives frequency agreement for the nonmethyl group modes comparable to that of the full force field. For the finite helices, it was supplemented with terms associated with the end groups (the CO_2^- group being taken as

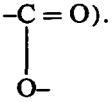

).

Lattice dynamics and density of states

Infinite helix

The calculation of the normal modes of vibration of an isolated, regular, infinite helix has been discussed extensively in the literature,[11] and we will not reproduce the details here. We recall that, as a result of the helical symmetry, the dimensions of the dynamical matrix can be reduced to the number of coordinates (Cartesian, internal, or symmetry) of one chemical repeat unit. It is convenient to display the phonon dispersion relation in the extended Brillouin zone (E.B.Z.), which is N times larger than the true B.Z., where N is the number of chemical repeat units in a crystallographic unit cell. In the E.B.Z., the phonon dispersion relation

[a)] This is paper no. 35 in a series on *Vibrational Analysis of Peptides, Polypeptides, and Proteins*. Paper no. 34 is Ref. 1.

 0021-9606/86/126989-08$02.10

has $3m$ branches (barring degeneracies), where m is the number of atoms in a chemical repeat unit.

The frequency distribution or phonon density of states from a branch of the dispersion relation, for a system periodic in one dimension (such as a helix), is[12]

$$g_s(\nu) = C\left.\frac{dk}{d\nu_s}\right|_{\nu_s=\nu}, \tag{1}$$

where $g_s(\nu)$ is the density of states at frequency ν from the sth branch ($s = 1,...,3m$), $\nu_s(\mathbf{k})$ is the phonon dispersion curve for the sth branch, $\mathbf{k}$ is the wave vector along the helix axis, and C is a normalization constant chosen so that

$$\int_0^\infty g_s(\nu)d\nu = 1. \tag{2}$$

The complete density of states is obtained by adding the contribution from each branch:

$$g(\nu) = \sum_{s=1}^{3m} g_s(\nu). \tag{3}$$

Finite helix

In the case of the finite helix, symmetry does not allow any reduction in the size of the dynamical matrix, and this matrix now involves the coordinates of all the atoms in the structure. In our computation, based on recently developed computer programs,[13] the dynamical matrix is set up in Cartesian coordinates; Wilson's GF method, which involves the "unnecessary" diagonalization of the G matrix, is particularly unsuitable in the present case owing to the large dimensions of the G matrix. In general, when the calculation for a finite system is done in Cartesian coordinates, the dynamical matrix is a symmetric band matrix, the bandwidth being determined by the longest interaction in the system, which in the present case is hydrogen bonding. The computation essentially has to be done by a "brute-force" method; techniques for efficiently setting up and diagonalizing such a dynamical matrix are described in Ref. 13.

The frequency distribution is obtained by scanning the normal mode spectrum with a small frequency interval (which we have taken to be 2 cm^{-1}) and directly counting the number of normal modes within each interval. The resulting distribution is normalized to one peptide residue.

An alternative numerical technique for computing the density of states is based on the negative eigenvalue theorem.[14,15] This method, which involves a determination of the number of frequencies in a specified interval, is computationally very efficient if the exact frequencies are not needed. However, if the frequencies are needed, the computational advantage is significantly reduced since the chosen frequency interval has to be narrowed considerably. The algorithm that we have used yields exact frequencies, since it was written with a view to investigating the influence of conformation on the normal mode frequencies of polypeptides and proteins.

Specific heat

In the harmonic approximation used here, the partition function separates into a product of contributions from each normal mode and the form of the specific heat is particularly simple. For a periodic lattice,[12]

$$C_V = \frac{1}{V}\frac{\partial}{\partial T}\sum_{\mathbf{k},s}\frac{h\nu_s(\mathbf{k})}{(e^{h\nu_s(\mathbf{k})/k_BT}-1)}, \tag{4}$$

where C_V is the specific heat at constant volume, V is the volume of the system, T is the temperature, h is Planck's constant, and k_B is Boltzmann's constant. The wave vector $\mathbf{k}$ is one dimensional in our calculation and lies along the axis of the helix. For a finite helix, $\mathbf{k}$ is not defined, and the sum in Eq. (4) is taken directly over the normal mode frequencies.

Going over to the continuum limit, Eq. (4) (or its analog for a finite system) can be rewritten as[12]

$$C_V = k_B\int_0^\infty g(\nu)\left[\frac{(h\nu/k_BT)}{\sinh(h\nu/k_BT)}\right]^2 d\nu, \tag{5}$$

where $g(\nu)$, the density of states, is normalized such that C_V is the heat capacity of a chemical repeat unit.

RESULTS AND DISCUSSION

Infinite helix: Phonon dispersion curves

The phonon dispersion curves obtained by using the α-helix force field of Dwivedi and Krimm[2] are shown in Fig. 1. The angle $\theta(=kh)$ is the phase difference between the vibrations of successive chemical units; the dispersion relation is plotted in one-half of the E.B.Z., which is 47 times larger than the true B.Z. The dispersion curves were obtained by solving the dynamical equation at an interval of $\theta = \pi/36$ in the positive half of the E.B.Z. ($0 \leqslant \theta \leqslant \pi$) and interpolating between the calculated points by using IMSL[16] interpolation routines. The optically active modes for a 47_{13} helix occur at $\theta = 0$ (A), $\theta = 26\pi/47$ (E_1), and $\theta = 52\pi/47$ (E_2), which are shown by dashed lines in the figure. (The E_2 mode is at $\theta = 42\pi/47$ in the figure owing to the periodicity of the dispersion relation.) The A and E_1 modes are infrared and Raman active, while the E_2 mode is Raman active only. There are four acoustic branches: in the E.B.Z. two of these occur at $\theta = 0$, and correspond to a translation along and rotation about the helix axis, and the remaining two occur at $\theta = 26\pi/47$, and correspond to translations perpendicular to the helix axis.

The effects of transition dipole coupling[17–19] have not been included in the calculations shown in Fig. 1. This is because the branches in which such effects are important are at frequencies which are too high to influence the specific heat in the temperature range where experiments have been performed ($T < 300$ K). Splittings due to transition dipole coupling were included in Ref. 2, and calculated frequencies show very good agreement with experiment.

In the E.B.Z., the dispersion relation has 30 branches corresponding to 30 degrees of freedom of the chemical repeat unit. Of these, branches (ν_{22},ν_{23}) and (ν_{28},ν_{29}), which correspond to CH_3 group vibrations, are doubly degenerate. For all the branches, the nature of the motions at the optically active points ($\phi = 0$, $26\pi/47$, $42\pi/47$) was described by the form of the potential energy distribution (PED) in Ref. 2. Eight branches arising from CH_3 group vibrations, ν_{14}, ν_{15}, ν_{21}, (ν_{22},ν_{23}), ν_{27}, and (ν_{28},ν_{29}), are essentially nondispersive. The nature of these vibrations, as determined from

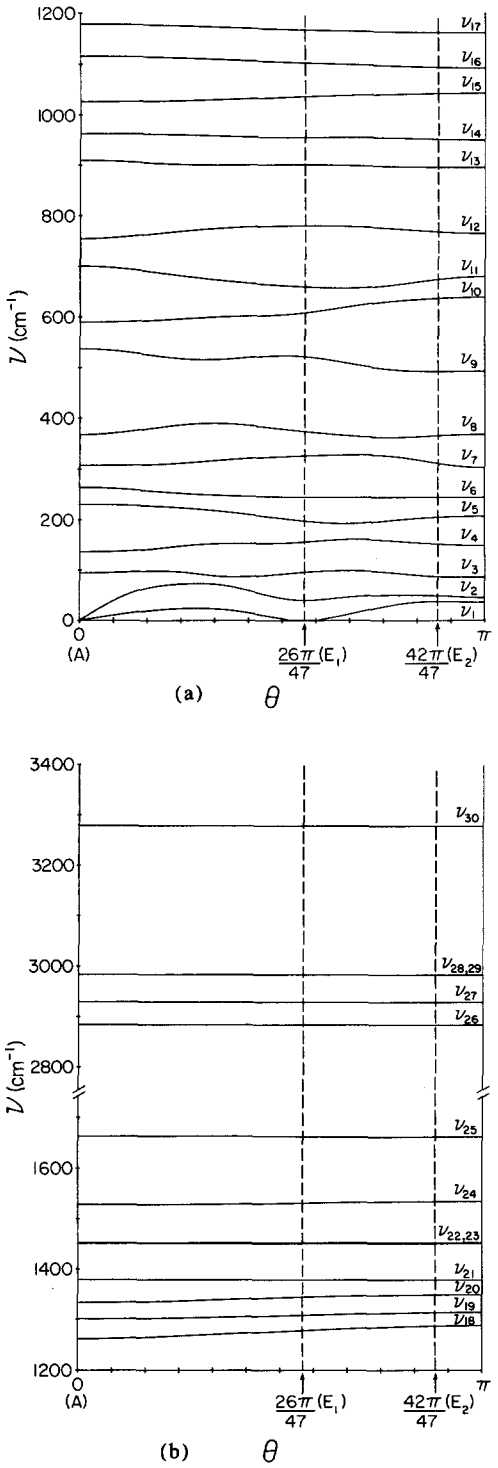

FIG. 1. Phonon dispersion curves for α-poly(L-alanine) in the extended Brillouin zone. (a) $\nu < 1200$ cm^{-1}. (b) $\nu > 1200$ cm^{-1}.

the form of the PED, is described in Ref. 2. In Table I we show the PED as a function of phase for branches ν_5 and ν_6, which contain the CH_3 torsion (t) mode (using previously defined local symmetry coordinates[20]). It can be seen from the PED that CH_3 t is coupled to a main-chain angle bending mode and cannot be treated as a localized mode. However, the side-chain point-mass approximation is valid for the other methyl branches which are not significantly affected by intrahelical interactions.

TABLE I. Potential energy distributions in methyl torsion branches of dispersion relations of α-poly(L-alanine).

Phase	Potential energy distribution[a]	
	ν_5	ν_6
0	$C^\alpha C^\beta$ t(63)	$C^\alpha C^\beta$ t(35) C^β b2(14)
$\pi/9$	$C^\alpha C^\beta$ t(57)	$C^\alpha C^\beta$ t(40) C^β b2(13)
$2\pi/9$	$C^\alpha C^\beta$ t(41)	$C^\alpha C^\beta$ t(56) C^β b2(10)
$3\pi/9$	$C^\alpha C^\beta$ t(22) C^β b2(11)	$C^\alpha C^\beta$ t(75)
$4\pi/9$	...	$C^\alpha C^\beta$ t(86)
$5\pi/9$	...	$C^\alpha C^\beta$ t(91)
$6\pi/9$	...	$C^\alpha C^\beta$ t(94)
$7\pi/9$	...	$C^\alpha C^\beta$ t(95)
$8\pi/9$	...	$C^\alpha C^\beta$ t(95)
π	...	$C^\alpha C^\beta$ t(94)

[a] Contributions $\geqslant 10\%$. t = torsion, b = bend (see Ref. 20 for definitions of local symmetry coordinates).

Infinite helix: Phonon density of states

In Fig. 2 we show the phonon density of states calculated from the dispersion relation shown in Fig. 1. The density of states is obtained as a histogram, since it was computed by sampling the phonon spectrum at an interval of 2 cm^{-1}. Although this discretization procedure leads to some smoothing of the singularities, the frequency interval chosen is sufficiently small so that it does not result in a distortion of the frequency spectrum.

In Table II we list the main peaks in the calculated phonon density of states below 650 cm^{-1}. Also shown in the table are the branches which gives rise to the peaks, the position in the B.Z. (phase) where a peak occurs, and the contributions to the PED at the peak from modes involving hydrogen atom motions. Since the incoherent scattering cross section for neutrons is much larger for hydrogen than for other atoms, peaks which have large contributions from hydrogen atom displacements will be the ones that appear in the INS cross section. Of the symmetry coordinates in this category shown in Table II, NH out-of-plane bend (ob) and CH_3 t probably make the largest contributions.

Although a direct comparison between the phonon density of states and the INS cross section is most easily done for a cubic lattice in the one-phonon approximation, which is clearly not valid in the present case, the PED allows us to make a qualitative comparison with the INS data. [In the case of polymers, where the cubic approximation does not hold, it has been shown[21] that it is useful to compute the eigenvector-weighted density of states, which can be compared directly with the INS data for oriented samples. In the present case, since no data are available on oriented samples of α-poly(L-alanine), we have not carried out such a calculation.] In the very low-frequency region, there are indications of possible peaks near 35,[3] 50,[3,7] and 60[3] cm^{-1}, the first two of which would be consistent with calculated peaks in the density of states at 37 and 50 cm^{-1} associated primarily with H···O stretch (s) and NH ob, respectively. A peak at 80

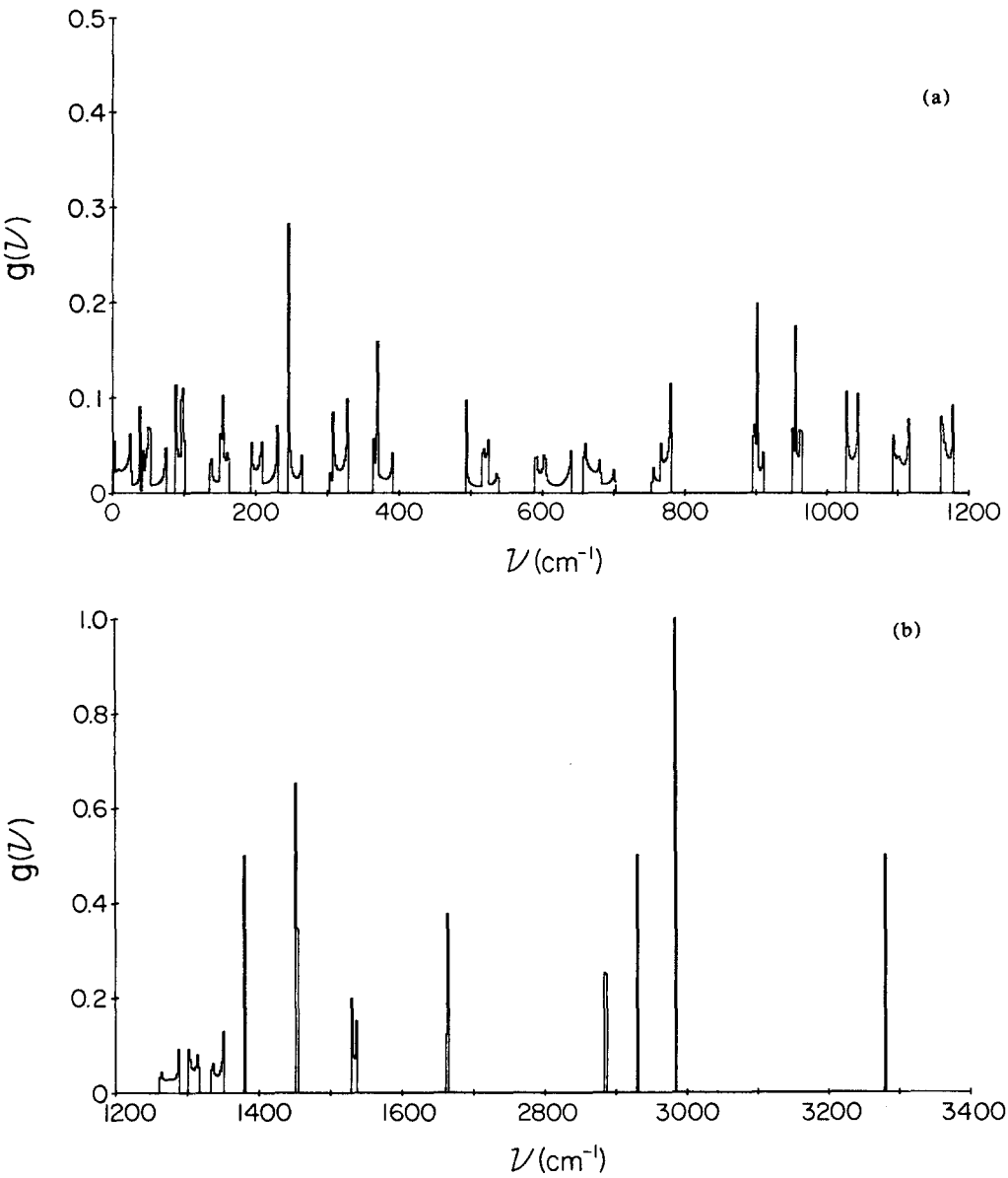

FIG. 2. Phonon density of states for α-poly(L-alanine). (a) $\nu < 1200$ cm^{-1}. (b) $\nu > 1200$ cm^{-1}.

cm^{-1} is clearly seen in the INS spectrum,[7] with the observation that there is "possibly a weak peak at about 100 cm^{-1}." [7] These are in agreement with calculated peaks at 87 (mainly NH ob) and 97 (H···O s) cm^{-1}; although both of these are of about equal magnitude in the density of states (see Fig. 2), it is understandable why the former should be stronger in the INS spectrum, since the NH ob contribution should result in larger hydrogen atom displacements. The observed peak[7] at 160 cm^{-1} is well assigned to calculated (NH ob) peaks at 153 and 159 cm^{-1}. The strong peak at 230,[3,7] with "a shoulder at about 200," [7] cm^{-1} is well accounted for by the structure of the CH_3 t peaks predicted at 245 and 229 cm^{-1}: both contain CH_3 t contributions, but the former is associated with a larger peak in the density of states (see Fig. 2) and a larger CH_3 t contribution to the PED (see Table I). [The high calculated frequencies, in the density of states as well as in the optical spectrum,[2] indicate that the $C^{\alpha}C^{\beta}$ t force constant in α-poly(L-alanine) should be slightly lower than that in β-poly(L-alanine), from which it was transferred without further refinement.] Finally, the (~ 600[3]) cm^{-1} is well correlated with calculated (mainly NH ob) peaks at 590 and 602 cm^{-1}. The force field is thus able to account quite satisfactorily for observed low-frequency peaks in the INS spectrum (improved experimental resolution would provide an even better test). This is most encouraging, since limited data on optical frequencies in this region made this a less secure part of the force field.

Infinite helix: Specific heat

The specific heat (C_V) of α-poly(L-alanine) obtained from the density of states of Fig. 2 is shown in the solid line of Fig. 3. (Note that 1 K = 0.695 cm^{-1}.) The solid and open circles show the experimental specific heat (C_P) of α- and β-poly(L-alanine), respectively, from the work of Daurel *et al.*,[8] and the dashed line is the calculation of Fanconi *et al.*[5] [Since the difference between C_P and C_V is usually very small for solids at low temperatures,[22] we have not converted C_V to C_P before comparing with experiment (the conversion, using Lindemann's relation, can itself give rise to errors

TABLE II. Calculated peaks in density of states, and observed peaks in inelastic neutron scattering spectrum, of α-poly(L-alanine).

Peak position (cm^{-1})					
Obs[a]	Calc	Branch	Potential energy distribution[b]		
	23	$\nu_1(5\pi/18)$	NH···O ib(28)	NH ob(25)	CO···H ib(10)
~35 vw[c]	37	$\nu_1(\pi)$	H···O s(12)	CO···H ib(11)	
~50 sh?	50	$\nu_2(15\pi/18)$	NH ob(45)	H···O s(34)	
	73	$\nu_2(5\pi/18)$	H···O s(32)	NH···O ib(10)	
80(5) m	87	$\nu_3(\pi)$	NH ob(50)	NH···O ib(24)	
~100 w	97	$\nu_3(3\pi/18)$	H···O s(33)		
	137	$\nu_4(0)$	···		
160(12) m	153	$\nu_4(7\pi/9)$	NH ob(42)		
	159	$\nu_4(2\pi/3)$	NH ob(26)		
	193	$\nu_5(2\pi/3)$	···		
	207	$\nu_5(\pi)$	···		
~200 sh	229	$\nu_5(0)$	$C^\alpha C^\beta$ t(63)		
230(19) s	245	$\nu_6(\pi)$	$C^\alpha C^\beta$ t(94)		
	263	$\nu_6(0)$	$C^\alpha C^\beta$ t(35)		
	307	$\nu_7(0)$	···		
	327	$\nu_7(11\pi/18)$	···		
	369	$\nu_8(0)$	NH ob(13)		
	389	$\nu_8(\pi/3)$	NH ob(21)		
	493	$\nu_9(\pi)$	···		
	523	$\nu_9(\pi/2)$	···		
580(70) m	590	$\nu_{10}(0)$	NH ob(36)	NH···O ib(11)	
	602	$\nu_{10}(8\pi/18)$	NH ob(24)		
	639	$\nu_{10}(\pi)$	NH ob(44)	NH···O ib(13)	

[a] From Ref. 7. Numbers in parentheses give resolution.
[b] Contributions $\geq 10\%$ from symmetry coordinates associated with motions of hydrogen atoms.
[c] From Ref. 3.

due to uncertainties in Lindemann's constant[22].] In the region $70 < T < 150$ K, our calculation shows better agreement with experiment than that of Fanconi *et al.*[5] Below 70 and above 150 K, both calculations give nearly identical results; for $T < 70$ K the experimental specific heat is lower than that predicted by theory, whereas above 150 K the experimental points rise sharply above the calculation.

The low-temperature discrepancy could arise from the presence of interhelical interactions, which have been neglected in our model. Our calculation was for an isolated helix, which is a one-dimensional system, and hence the specific heat varies as T at low temperatures. In a real system, interhelical interactions, though small, are present and contribute to the lattice modes; this modifies the density of states and leads to a three-dimensional T^3 behavior of the low-temperature specific heat. In trying to fit a Tarasov function[22] to the experimental specific heat, Daurel *et al.*[8] found that a 1–3 Tarasov function gives a good fit up to 100 K.

Another source of error in the low-temperature region is that our force field, which was obtained at room temperature, does not take into account anharmonic effects such as the expansion of the lattice, which to first order lead to a linear decrease in frequency with increasing temperature. These effects are particularly important in the low-frequency region, where our temperature-independent force field predicts lower frequencies and consequently leads to an overestimation of the specific heat.

The sharp rise in the specific heat above 150 K is harder to understand. It could arise from the presence of defects or impurities, or it could be due to anharmonicities. It was suggested to us[23] that water may be present in the sample, and could influence its specific heat around 150 K.[24] We therefore recalculated the specific heat assuming one molecule of absorbed water/peptide residue, and taking the librational frequenices of water to be 450, 550, and 720 cm^{-1}. (These values, taken from Ref. 24, are rough estimates chosen only to get an idea of the trend in the specific heat.) The result is shown by the dotted curve of Fig. 3. In spite of the fact that the concentration of water was taken to be (probably unrea-

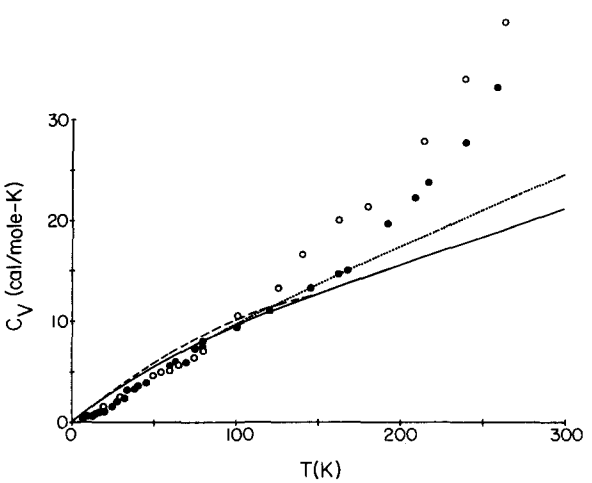

FIG. 3. Specific heat of α-poly(L-alanine). — C_V, present calculation; - - - C_V, Fanconi *et al.* (Ref. 5); ··· C_V, present calculation with one molecule of H_2O/peptide residue. The solid and open circles show the experimental data of Daurel *et al.* (Ref. 8) for α- and β-poly(L-alanine), respectively.

sonably) high, we see that the rise in the specific heat falls far short of the experimental trend. This calculation also shows that, if the observed rise in the specific heat does come from localized modes arising from defects or impurities, the concentration of such defects or impurities must be rather large.

It is more likely that anharmonicity in the methyl torsion mode, which is weakly coupled to the main chain, leads to the rise in C_P. Examination of the specific heats of poly(glycine),[25] poly(L-alanine),[8] and poly(L-valine)[26] indicates a systematic effect attributable to methyl groups. A graphic compilation of these specific heats[27] shows that, despite differences in conformation and intermolecular bonding, the C_P of poly(glycine)I is similar to that of poly(glycine)II, and the C_P of α-poly(L-alanine) is similar to that of β-poly(L-alanine). However, poly(L-alanine), which differs from poly(glycine) by the presence of a side-chain CH_3 group, has a C_P larger than that of poly(glycine), the deviation setting in at $\sim$150 K, and β-poly(L-valine), which has two side-chain CH_3 groups, shows an even greater deviation from the C_P of poly(glycine). In both cases, the deviation is far greater than can be accounted for by harmonic contributions arising from the additional degrees of freedom introduced by the methyl group.

A starting approximation to compute anharmonic effects is to treat the CH_3 group as an independent single-particle rotor. The subject of single-particle rotations in molecular crystals has been reviewed in a recent book.[28] In the Appendix we outline a calculation along the lines of Pitzer and Gwinn,[29] which treats the CH_3 group as a single rotor in a threefold symmetric potential. As we might expect, the predicted increase in C_V due to anharmonicity in this simplified model is far less than the deviation seen by Daurel *et al.*[8] However, couplings between methyl torsion and main-chain modes, or between methyl groups, could lead to a significant enhancement of the specific heat. In α-poly(L-alanine), such CH_3–CH_3 interactions have been invoked to explain a splitting in the CH stretch mode.[30] While more elaborate models are clearly needed, the highly simplified calculation in the Appendix shows the plausibility of specific heat enhancement due to anharmonicity in the methyl torsion mode.

Finite helix: Frequency distribution and specific heat

The frequency distributions and the specific heats of finite helices of varying lengths are shown in Figs. 4 and 5. Also shown in the figures are the corresponding quantities for the infinite helix in the side-chain point-mass approximation. In the latter case, the density of states, except for the CH_3 modes, is quite similar to that for the full calculation (cf. Fig. 2). The density of states in the frequency region above 800 cm^{-1} converges quite rapidly, so that by 15 residues the vibrational spectrum is essentially identical to that of an infinite helix. The convergence in the low-frequency region is much slower, and a helix of 25 residues still has a specific heat in the low-temperature region significantly higher than that of an infinite helix. We plan further studies to characterize the normal modes and infrared intensities[31] of such finite helices.

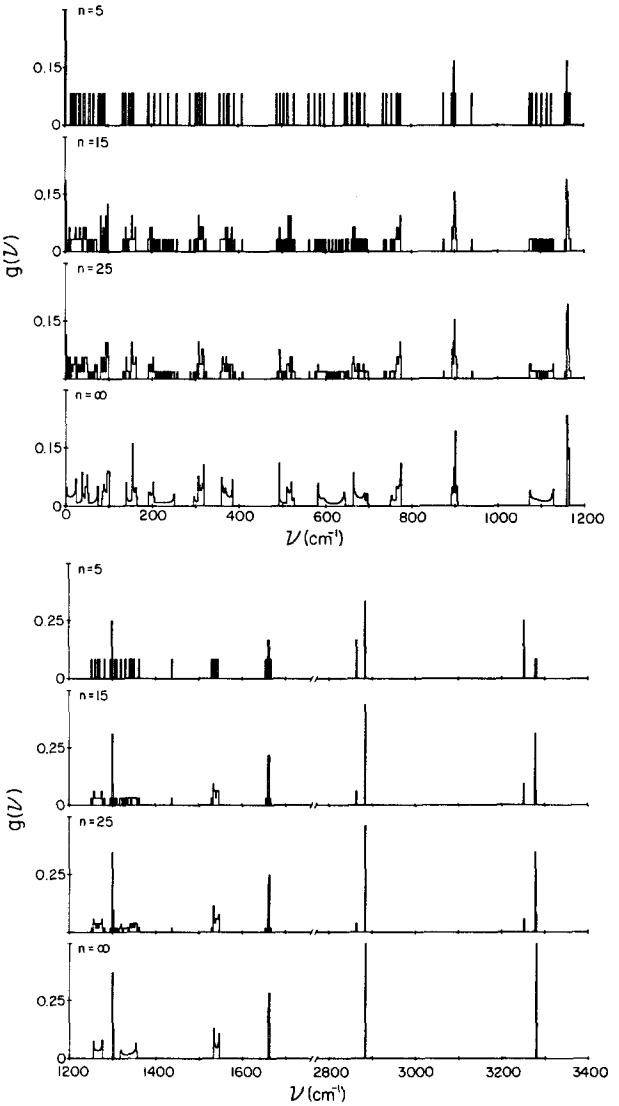

FIG. 4. Frequency distributions for finite helices of $n = 5,15,25$ peptide residues and for the infinite helix, in the side-chain point-mass approximation.

CONCLUDING REMARKS

Two main results emerge from our calculation: (i) The force field of Dwivedi and Krimm[2] for α-poly(L-alanine) not only gives better agreement with observed optical fre-

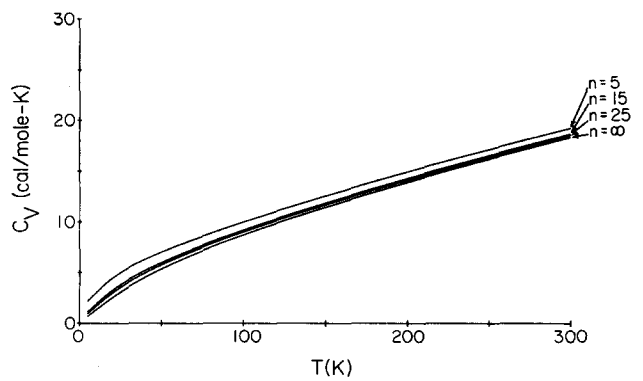

FIG. 5. Specific heat of finite helices of $n = 5,15,25$ residues and of the infinite helix, in the side-chain point-mass approximation.

quencies than earlier force fields, but also leads to improved agreement with neutron scattering and specific heat ($T<150$ K) data. (ii) With the exception of the methyl torsion mode, the dynamics of the α-helix is well approximated by the side-chain point-mass model if a suitably refined force field is used.

A systematic trend seen in the specific heat data for polypeptides[27] suggests that the enhancement in the observed specific heat for $T>150$ K arises from anharmonicity in the methyl torsion mode. Further experimental and theoretical work are required to test this suggestion. Experimentally, calorimetric data at higher temperatures are needed to characterize the nature of the specific heat anomaly, while theoretically, more realistic models of anharmonicity which include mode–mode couplings need to be developed.

ACKNOWLEDGMENTS

We thank Dr. Jagdeesh Bandekar and Dr. Toon C. Cheam for many helpful general discussions, and Professor George Summerfield for discussions about neutron scattering cross sections. This work was supported by NSF grants DMR-8303610 and PCM-8214064.

APPENDIX

The simplest model for methyl group rotation is to treat the methyl group as an independent rigid rotor in a threefold symmetric potential, $V(\theta) = V_0/2\ (1-\cos 3\theta)$, where θ is the angle of rotation and V_0 is the height of the barrier separating potential minima. The eigenfunctions of Schrödinger's equation corresponding to this potential are the Mathieu functions; the exact energy eigenvalues and the partition function for this model have been obtained by Pitzer and Gwinn.[29] While in principle this calculation is straightforward, the partition function cannot be evaluated analytically and hence the thermodynamic functions are not easily visualized. Instead of computing the specific heat using the exact partition function, we present below an approximation which allows a closed form evaluation of the partition function. (This approximation has been suggested in Pitzer's paper; however, there is a sign error in the expression for C_V.)

If the potential is such that the lowest two eigenvalues are close to the corresponding harmonic oscillator energy levels the partition function Z is well approximated by

$$Z = Z^{\mathrm{cl}}[Z^{\mathrm{QHO}}/Z^{\mathrm{CHO}}], \tag{A1}$$

where Z^{cl} is the full classical partition function, while Z^{QHO} and Z^{CHO} are the quantum and classical partition functions, respectively, corresponding to the harmonic oscillator Hamiltonian, i.e., $V = 9V_0\theta^2/4$ [clearly Eq. (A1) leads to the right low- and high-temperature limits: as $T\to 0$, $Z\to Z^{\mathrm{QHO}}$, and as $T\to\infty$, $Z\to Z^{\mathrm{cl}}$].

Since

$$C_V = k_B\beta^2\left(\frac{\partial^2 \ln Z}{\partial\beta^2}\right)$$

($\beta = 1/k_BT$), Eq. (A1) implies

$$C_V = C_V^{\mathrm{cl}} + C_V^{\mathrm{QHO}} - C_V^{\mathrm{CHO}}, \tag{A2}$$

where the superscript QHO (CHO) stands for a quantum (classical) harmonic oscillator. Thus, the deviation of the specific heat from that of a quantum harmonic oscillator is

$$C_V - C_V^{\mathrm{QHO}} = C_V^{\mathrm{cl}} - C_V^{\mathrm{CHO}} = C_V^{\mathrm{cl}} - k_B. \tag{A3}$$

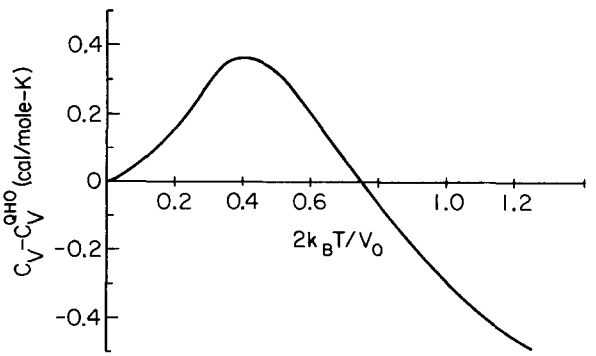

FIG. 6. Difference between C_V of a rigid rotor in a threefold symmetric potential and that of a quantum harmonic oscillator, as a function of dimensionless temperature.

We proceed now to obtain Z^{cl} and C_V^{cl}. The Hamiltonian $\mathscr{H}$ of the system is

$$\mathscr{H} = \frac{P_\theta^2}{2I} + \frac{V_0}{2}(1-\cos 3\theta), \tag{A4}$$

where P_θ is the momentum conjugate to the angle of rotation θ, and I is the moment of inertia about the axis of rotation. Then

$$Z^{\mathrm{cl}} = \frac{1}{h}\int\int e^{-\mathscr{H}/k_BT}d\theta\, dP_\theta$$

$$= \frac{1}{h}\sqrt{2\pi Ik_BT}\,e^{-V_0/2k_BT}2\pi I_0\left(\frac{V_0}{2k_BT}\right), \tag{A5}$$

where h is Planck's constant, and I_0 is the modified Bessel function of zero order.[32] The corresponding specific heat is

$$C_V^{\mathrm{cl}} = \frac{k_B}{2} + k_Bx^2 - k_Bx\frac{I_1(x)}{I_0(x)} - k_B\left(\frac{xI_1(x)}{I_0(x)}\right)^2, \tag{A6}$$

where $x = V_0/2k_BT$. [The sign of the third term on the right-hand side of Eq. (A6) differs from that of Pitzer and Gwinn.] At high temperatures ($x\to 0$), $C_V^{\mathrm{cl}}\to k_B/2$, which is the specific heat of a classical free rotor, while at low temperature ($x\to\infty$) we see (using the asymptotic expansion for the modified Bessel functions[33]) that $C_V^{\mathrm{cl}}\to k_B$, which is the specific heat of a classical harmonic oscillator. Figure 6 is a plot of $C_V - C_V^{\mathrm{QHO}}$ as a function of temperature using values of $I_0(x)$ and $I_1(x)$ from Refs. 33–35.

If the barrier height V_0 is known, then Fig. 6 allows us to estimate the temperature at the peak in C_V: $T_{\mathrm{peak}}\cong 0.4\ V_0/2k_B$. V_0 can in turn be estimated from the methyl torsion fundamental, ν_T, assuming that this corresponds to the fundamental of the harmonic approximation to Eq. (A4), i.e.,

$$\nu_T^2 = \frac{9V_0}{8\pi^2c^2I}, \tag{A7}$$

where c is the velocity of light. For α-poly(L-alanine), taking $\nu_T = 230\ \mathrm{cm}^{-1}$, and $I = 3.17$ amu Å^2 (assuming the

methyl group to be a free rotor attached to an infinite mass), we get $V_0 = 13.2$ kJ/mol and $T_{peak} = 318$ K.

[1]V. M. Naik and S. Krimm, Biophys. J. (in press).
[2]A. M. Dwivedi and S. Krimm, Biopolymers **23**, 923 (1984).
[3]M. V. Krishnan and V. D. Gupta, Chem. Phys. Lett. **6**, 231 (1970).
[4]K. Itoh and T. Shimanouchi, Biopolymers **9**, 383 (1970).
[5]B. Fanconi, W. E. Small, and W. L. Peticolas, Biopolymers **10**, 1277 (1971).
[6]V. D. Gupta, H. Boutin, and S. Trevino, Nature **214**, 1325 (1967).
[7]W. Drexel and W. L. Peticolas, Biopolymers **14**, 715 (1975).
[8]M. Daurel, P. Delhaes, and E. Dupart, Biopolymers **14**, 801 (1975).
[9]S. Arnott and S. D. Dover, J. Mol. Biol. **30**, 209 (1967).
[10]A. M. Dwivedi and S. Krimm, J. Phys. Chem. **88**, 620 (1984).
[11]In the case of a helix, the wave vector lies along the screw-symmetry axis, and hence the dynamical matrix can be factored at all points in the Brillouin zone. Thus, the formalism at $\mathbf{k} = 0$ is valid for all $\mathbf{k}$. A representative article that describes the calculation of the optically active normal modes using the GF method is H. Sugeta and T. Miyazawa, J. Chem. Phys. **47**, 2034 (1967). While it is computationally efficient to perform the calculation using Cartesian coordinates, the normal modes are more easily visualized from the potential energy distribution in local symmetry coordinates. Hence our computations were done using the traditional GF method as described in the above article.
[12]N. W. Ashcroft and N. D. Mermin, *Solid State Physics* (Holt, Reinhart, and Winston, Philadelphia, 1976).
[13]S. Ataka and M. Tasumi, J. Mol. Struct. (in press). An earlier version, which does not include hydrogen bonds, was used by M. Tasumi, H. Takeuchi, S. Ataka, A. M. Dwivedi, and S. Krimm, Biopolymers **21**, 711 (1982).
[14]P. Dean, Rev. Mod. Phys. **44**, 127 (1972).
[15]G. Zerbi, in *Advances in Infrared and Raman Spectroscopy* (Wiley, New York, 1984), Vol. 11.
[16]*International Mathematical and Statistical Library*, Vol. 2, Chap. I, Interpolation Routines, 1984.
[17]S. Krimm and Y. Abe, Proc. Natl. Acad. Sci. U.S.A. **69**, 2788 (1972).
[18]W. H. Moore and S. Krimm, Proc. Natl. Acad. Sci. U.S.A. **72**, 4933 (1975).
[19]T. C. Cheam and S. Krimm, Chem. Phys. Lett. **107**, 613 (1984).
[20]W. H. Moore and S. Krimm, Biopolymers **15**, 2465 (1976).
[21]J. E. Lynch, G. C. Summerfield, L. A. Feldkamp, and J. S. King, J. Chem. Phys. **48**, 912 (1968).
[22]E. S. R. Gopal, *Specific Heats at Low Temperatures* (Plenum, New York, 1966).
[23]L. Finegold (private communication).
[24]D. Eisenberg and W. Kauzmann, *The Structure and Properties of Water* (Oxford University, Oxford, 1969).
[25]L. Finegold and P. K. Kumar, Thermochim. Acta **48**, 51 (1981).
[26]M. Daurel, P. Delhaes, and P. Dupart, Biopolymers **15**, 415 (1976).
[27]U. Gaur and B. Wunderlich, J. Phys. Chem. Ref. Data **12**, 65 (1985).
[28]W. Press, *Single Particle Rotations in Molecular Physics* (Springer, New York, 1981).
[29]K. S. Pitzer and W. D. Gwinn, J. Chem. Phys. **10**, 428 (1942).
[30]J. F. Rabolt, W. H. Moore, and S. Krimm, Macromolecules **10**, 1065 (1977).
[31]T. C. Cheam and S. Krimm, J. Chem. Phys. **82**, 1631 (1985).
[32]I. S. Gradshteyn and I. M. Ryzhik, *Table of Integrals, Series, and Products* (Academic, New York, 1980).
[33]*Bessel Functions*, BAAS Mathematical Tables (Cambridge University, Cambridge, 1950), Vol. 6.
[34]L. J. Briggs and A. N. Lowan, *Table of the Bessel Functions $J_0(z)$ and $J_1(z)$ for Complex Arguments* (Columbia University, New York, 1943).
[35]L. Fox, *A Short Table for Bessel Functions of Integer Orders and Large Arguments* (Cambridge University, Cambridge, 1954).